



# Transient behavior of imperfect bi-directional functionally graded sandwich plates under moving loads

M. Esmailzadeh<sup>1</sup> · M. E. Golmakani<sup>2</sup> · Y. Luo<sup>1</sup> · M. Bodaghi<sup>3</sup>

Received: 28 November 2020 / Accepted: 4 October 2021  
© The Author(s) 2021

## Abstract

An investigation of dynamic behaviors of a sandwich plate containing an imperfect two dimensional functionally graded (2D-FG) core surrounded by two faces on a two-parameter elastic foundation and subjected to a moving load is carried out in this paper. The present sandwich solid is composed of a porous 2D-FG core covered by two homogenous layers. It is assumed that the middle layer has micro voids dispersed uniformly and unevenly through the layer thickness. The fundamental equations are governed within the framework of first-order-shear deformation theory by utilizing Hamilton's principle, von-Karman geometrical nonlinearity and the principal of mixtures. Newmark direct integration procedure is implemented to transform the dynamic equations into a static form and then the kinetic dynamic relaxation numerical technique in conjunction with the finite difference discretization method are employed to solve the nonlinear partial differential governing equations. Finally, the effects of porosity fraction and scattering patterns, boundary constrains, the variation of materials' grading indexes and elastic foundation constants on the transient performances of the plate are studied in detail.

**Keywords** 2D-FG sandwich plate · Porosity · Moving load · Kinetic dynamic relaxation · Newmark technique

## 1 Introduction

A sandwich structured composite is an advanced type of composite materials usually fabricated by attaching two fairly thin but strong face sheets to a relatively thick light-weight core [1]. Using a first order shear deformation theory and Hamilton's principle, Karroubi and Irani Rahaghi [2] performed a study on the free vibration of a three-layer rotating shell which consists of a functionally graded core and two piezoelectric face sheets. The emphasis of the current study is on the time-dependent deflection of a sandwich plate made of a porous plate whose materials functionally scattered along thickness and in-plane directions as a core solid with two similar homogenous faces.

In the few recent decades, more and more craftsmen have tried to seek for advanced materials which have more capacity to resist both different mechanical loadings and sever environmental conditions [3, 4]. This way, 2D-FG solids have attracted enormous attentions from both research and industrial divisions [5]. Scientists have showed that functionally graded materials with two directional dependent materials properties have more resistance against severe temperature variations compared to one-dimensional (1D) functionally graded materials (FGMs) [6–8]. Beferani et al. [9] analyzed the vibrational characteristics of functionally graded plates on Winkler and Pasternak foundations. Sheikholeslami and Saidi [10] showed the impacts of some factors such as the thickness ratio and elastic foundation parameters on the natural frequencies of thick functionally graded rectangular plates. Some years later, Chen et al. [11] explored the effects of several factors such as geometric features and material parameters on the vibrational behaviors of cylindrical 2D-FG shells. The vibrational and buckling performances of 2D-FG beams were analyzed by Nguyen and Lee [12]. Using the generalized differential quadrature method, Fariborz and Batra [13] studied the free vibration of curved beams with two directional material properties. Tang and Ding [14] used Euler–Berlioni theory along with

✉ M. Bodaghi  
mahdi.bodaghi@ntu.ac.uk

<sup>1</sup> Department of Mechanical Engineering, University of Manitoba, Winnipeg, MB, Canada

<sup>2</sup> Department of Mechanical Engineering, Mashhad Branch, Islamic Azad University, Mashhad, Iran

<sup>3</sup> Department of Engineering, School of Science and Technology, Nottingham Trent University, Nottingham NG11 8NS, UK

the von Kármán scheme for large deflections to investigate the effects of material gradients on the mechanical characteristics of 2D-FG beams under hygro-thermal loads. The nonlinear vibrational behaviors of pre- and post-buckled nonuniform bi-directional functionally graded microbeams under nonlinear thermal loading were investigated by Attia and Mohamed [15]. In another study, Saini and Lal [16] analyzed the free vibrational behavior of functionally graded moderately thick circular plates with two-dimensional material and temperature distribution.

During the fabrication of functionally graded materials, micro-voids can be created inside the FGMs. For instance, porosity formation can be a result of mixing some materials with different sintering temperature [17]. Wang et al. [18] investigated the thermal vibration of a cylindrical shell with structural defections dispersed monotonously or functionally through the thickness path. Zhou et al. [19] conducted a study on the vibrational and flutter behaviors of functionally graded plates containing porosities. Esmailzadeh and Kadhodayan [20] used the kinetic dynamic relaxation technique combined with Newmark approach to undertake a numerical study on nonlinear dynamic behaviors of porous stiffened 2D-FG sheets. Following that, they [21] investigated the effects of porosity configurations on time-dependent behavior of bi-layer sandwich plates.

The numerical replicas of structures which rest on elastic foundations are frequently employed to duplicate numerous real models in industrial sectors. In several cases, an elastic medium can be assumed as simple instruments such as spring. Beferani and Saidi [22] used the third order shear deformation plate theory along with the Levy approach to investigate the buckling and vibrational behaviors of symmetrically laminated thick rectangular plates supported by elastic foundations. In another research, Gao et al. [23] presented the effects of some factors such as damping ratios and temperature changes on the dynamic performance of composite orthotropic plates resting on an elastic medium.

Structures subjected to moving loads can be seen in various applications such as trains on the track, airplanes passing floating airports, machine tools, etc. From a computational point of view, the travelling load is usually applied as a simple massless force or an oscillator or an inertial force. Numerous historical studies concerning the moving load problem exist in the open literatures [20, 24–27]. Simsek [28] conducted a study on nonlocal vibration of a single-walled carbon nanotube carrying a moving harmonic load. The nonlocal elasticity theory was used by Chang [29] and Nami and Janghorban [30], respectively, to study dynamic behaviors of double-walled nanotubes and nanoplates.

Shahsavari and Janghorban [31] also investigated dynamic deflections and shearing responses of nanoplates under moving loads using the nonlocal theory. With the consideration of nano-system coefficients, Barati et al. [32] undertook a research on transient responses of nanobeams under inertia forces. Recently, stability of graphite sheets resting on elastic foundations and subjected to moving nanoparticles was investigated by Pirmoradian et al. [33].

Based on the comprehensive literature review conducted by the authors, on the basis of the FSDT, there is no numerical study on the nonlinear dynamic behaviors of sandwich rectangular plates with porous 2D-FG core mounted on elastic foundations and under the action of moving loads. In this study, a 2D-FG core is assumed to be defected with porosity inclusions uniformly or functionally distributed through its thickness. Hamilton's principle in conjunction with von-Karman theory are used to derive the time-dependent equations, and then an amalgamation of kinetic dynamic relaxation method and Newmark implicit integration are employed for solving governing equations. Eventually, the influence of some key parameters including elastic foundations, material gradient properties, boundary constrains, and moving load on transient responses of the sandwich plate are precisely scrutinized. The result of this research work can be applied to bridging engineering and transportation divisions, where dynamic effects of the moving vehicles on bridge structures can play a significant role on their lifetime.

## 2 Theoretical modelling

Consider a rectangular sandwich plate with length  $a$ , width  $b$  and thickness  $h (= h_c + 2h_f)$  along  $x$ ,  $y$  and  $z$  directions, respectively, as shown in Fig. 1. This plate rests on an elastic foundation and is exposed to a moving load. Subscripts  $c$  and  $f$  denote the core layer and face surfaces, respectively.

### 2.1 Bi-directional FG plate with geometrical imperfections

Figure 1 shows that the mixture of the 2D-FG core changes along both  $x$  and  $z$  directions. The upper surface of the plate,  $h_c/2$ , is completely made out of material 3, then its mechanical properties vary to a composition of material 1 and 2 at the bottom of the sheet. The plate's mechanical properties change along axial direction at  $z = -h_c/2$ , as well, from pure material 1 at  $x=0$  to unadulterated ceramic 2 at  $x=a$ .

The effective mechanical properties,  $P(x, z)$ , of the 2D-FG core with even micro-void inclusions (Fig. 2a) based on the rule of mixtures can be measured by [20]

**Fig. 1** Schematic of a sandwich plate resting on an elastic foundation under a moving load

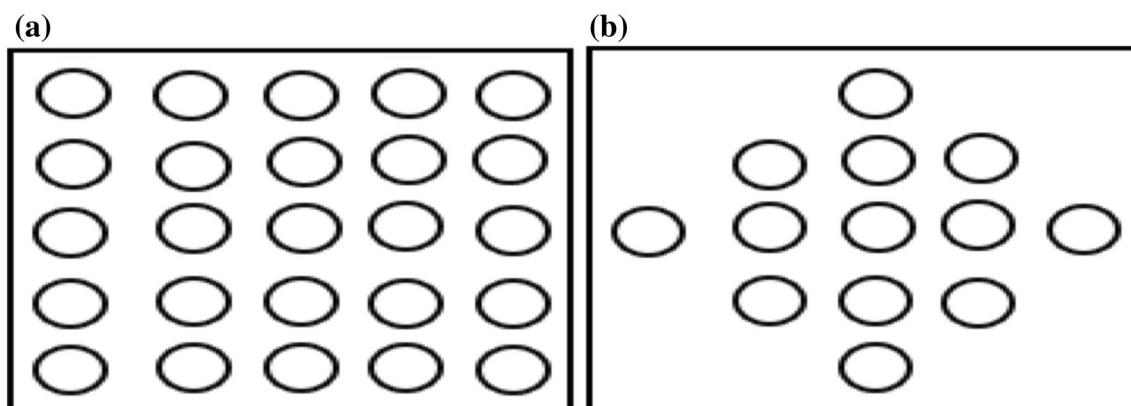
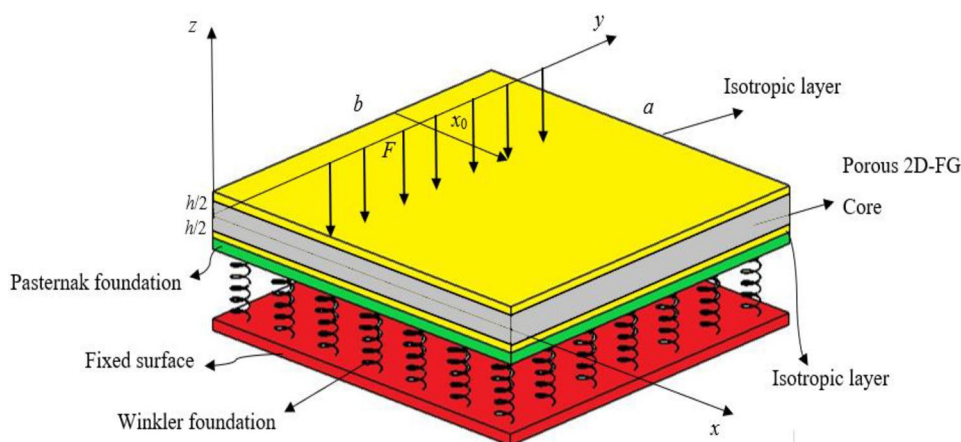


**Fig. 2** Two types of porosity distributions through the plate thickness

$$P(x, z) = P_1 \left( 1 - \left( \frac{z}{h_c} + \frac{1}{2} \right)^n \right) \left( 1 - \left( \frac{x}{a} \right)^m \right) + P_2 \left( 1 - \left( \frac{z}{h_c} + \frac{1}{2} \right)^n \right) \left( \frac{x}{a} \right)^m + P_3 \left( 1 - \left( \frac{z}{h_c} + \frac{1}{2} \right)^n \right) - \frac{\alpha}{2} (P_1 + P_2 + P_3), \tag{1}$$

where  $P_1, P_2$  and  $P_3$  are, respectively, mechanical properties (Young’s modulus ( $E$ ), and mass density ( $\rho$ )) of materials 1, 2 and 3, and also positive parameters  $n$  and  $m$  are gradient indexes along  $z$ - and  $x$ -axes. In the case of the core with uneven porosities (Fig. 2b), the effective mechanical properties become [20]:

$$P(x, z) = P_1 \left( 1 - \left( \frac{z}{h_c} + \frac{1}{2} \right)^n \right) \left( 1 - \left( \frac{x}{a} \right)^m \right) + P_2 \left( 1 - \left( \frac{z}{h_c} + \frac{1}{2} \right)^n \right) \left( \frac{x}{a} \right)^m + P_3 \left( 1 - \left( \frac{z}{h_c} + \frac{1}{2} \right)^n \right) - \frac{\alpha}{2} (P_1 + P_2 + P_3) \left( 1 - \frac{2|z|}{h_c} \right), \tag{2}$$

where  $P(x, z)$  represents Young’s modulus ( $E$ ), and mass density ( $\rho$ ). Also,  $\alpha$  denotes porosity fraction. The Poisson’s ratio ( $\nu$ ) is assumed to be constant.

### 2.2 Fundamental equations

Because the main aim of the current study is to investigate dynamic response of moderately thick sandwich plates, equivalent single layer theory of the first-order shear deformation is hired to describe the kinematics of deformation

of the plate. The FSDT provides a sufficiently accurate description of global response for moderately thick layered structures with complex constitutive behavior [34]. Based on FSDT along with von-Karman nonlinearity, the

stress–displacement relationships of face layers and a porous 2D-FGM core are written as follows:

$$\begin{Bmatrix} \sigma_{xx} \\ \sigma_{yy} \\ \sigma_{xy} \\ \sigma_{yz} \\ \sigma_{xz} \end{Bmatrix}_c = \begin{bmatrix} Q_{11} & Q_{12} & 0 & 0 & 0 \\ Q_{12} & Q_{11} & 0 & 0 & 0 \\ 0 & 0 & Q_{66} & 0 & 0 \\ 0 & 0 & 0 & C_{44} & 0 \\ 0 & 0 & 0 & 0 & C_{55} \end{bmatrix}_c \times \begin{Bmatrix} \frac{\partial u}{\partial x} + \frac{1}{2} \left( \frac{\partial w}{\partial x} \right)^2 \\ \frac{\partial v}{\partial y} + \frac{1}{2} \left( \frac{\partial w}{\partial y} \right)^2 \\ \frac{\partial u}{\partial y} + \frac{\partial v}{\partial x} + \frac{\partial w}{\partial x} \frac{\partial w}{\partial y} \\ \psi_y + \frac{\partial w}{\partial y} \\ \psi_x + \frac{\partial w}{\partial x} \end{Bmatrix} + z \begin{Bmatrix} \frac{\partial \psi_x}{\partial x} \\ \frac{\partial \psi_y}{\partial y} \\ \frac{\partial \psi_x}{\partial y} + \frac{\partial \psi_y}{\partial x} \\ 0 \\ 0 \end{Bmatrix} \quad (3a)$$

$$\begin{Bmatrix} \sigma_{xx} \\ \sigma_{yy} \\ \sigma_{xy} \\ \sigma_{yz} \\ \sigma_{xz} \end{Bmatrix}_f = \begin{bmatrix} Q_{11} & Q_{12} & 0 & 0 & 0 \\ Q_{12} & Q_{11} & 0 & 0 & 0 \\ 0 & 0 & Q_{66} & 0 & 0 \\ 0 & 0 & 0 & C_{44} & 0 \\ 0 & 0 & 0 & 0 & C_{55} \end{bmatrix}_f \times \begin{Bmatrix} \frac{\partial u}{\partial x} + \frac{1}{2} \left( \frac{\partial w}{\partial x} \right)^2 \\ \frac{\partial v}{\partial y} + \frac{1}{2} \left( \frac{\partial w}{\partial y} \right)^2 \\ \frac{\partial u}{\partial y} + \frac{\partial v}{\partial x} + \frac{\partial w}{\partial x} \frac{\partial w}{\partial y} \\ \psi_y + \frac{\partial w}{\partial y} \\ \psi_x + \frac{\partial w}{\partial x} \end{Bmatrix} + z \begin{Bmatrix} \frac{\partial \psi_x}{\partial x} \\ \frac{\partial \psi_y}{\partial y} \\ \frac{\partial \psi_x}{\partial y} + \frac{\partial \psi_y}{\partial x} \\ 0 \\ 0 \end{Bmatrix}, \quad (3b)$$

in which  $u$ ,  $v$  and  $w$  are, respectively, the displacements of the sandwich plate along  $x$ ,  $y$  and  $z$  directions. Also  $\psi_x$  and  $\psi_y$  denote angular dislocations about  $y$  and  $x$  axes. The plane stress-reduced stiffness coefficients ( $Q_{ij}$ ) of the ceramic's layers ( $f$ ) and porous 2D-FG core ( $c$ ) are respectively defined as follows [21]:

$$\text{Face : } \begin{cases} Q_{11} = \frac{E_f}{1 - \nu_f^2} \\ Q_{12} = \frac{\nu_f E_f}{1 - \nu_f^2} \\ C_{44} = C_{55} = Q_{66} = G_f = \frac{E_f}{2(1 + \nu_f)} \end{cases} \quad (4)$$

$$\text{Core: } \begin{cases} Q_{11} = \frac{E_c(x, z)}{1 - \nu_c^2} \\ Q_{12} = \frac{\nu_c E_c(x, z)}{1 - \nu_c^2} \\ C_{44} = C_{55} = Q_{66} = G_c(x, z) = \frac{E_c(x, z)}{2(1 + \nu_c)} \end{cases},$$

$\nu_f$  and  $\nu_c$  are, respectively, the Poisson's ratios of the face sheets and the core. The stress resultants and moments are defined as [35]:

$$(N_i, M_i) = \int_{h_c/2}^{h_c/2+h_f} ((1, z)\sigma_i)_f dz + \int_{-h_c/2}^{h_c/2} ((1, z)\sigma_i)_c dz + \int_{-(h_c/2+h_f)}^{-h_c/2} ((1, z)\sigma_i)_f dz, \quad (i = xx, yy, xy)$$

$$Q_i = K^2 \left( \int_{h_c/2}^{h_c/2+h_f} (\sigma_{iz})_f dz + \int_{-h_c/2}^{h_c/2} (\sigma_{iz})_c dz + \int_{-(h_c/2+h_f)}^{-h_c/2} (\sigma_{iz})_f dz \right), \quad (i = x, y), \quad (5)$$

$K^2$  represents the transverse shear correction constant and is set as 0.833.

To derive the fundamental equations, the Hamilton's principle is used as,

$$\int_0^T (\delta T + \delta W - \delta K) dt = 0, \quad (6)$$

where  $\delta T$  is the variation of strain energy and also  $\delta W$ , and  $\delta K$  are, separately, the variation of applied work and kinetic energy of a mechanism.  $\delta T$  can be expressed in terms of stress and strain as:

$$\delta T = \iiint_V \delta t dV = \iiint_V \sigma_{ij} \delta \epsilon_{ij} dV. \quad (7)$$

The variation of kinetic energy can be expressed by:

$$\delta K = \iiint_V (\rho_f + \rho_c(x, z)) ((u + z\psi_x)\delta(\dot{u} + z\dot{\psi}_x) + (v + z\psi_y)\delta(\dot{v} + z\dot{\psi}_y) + \dot{w}\delta\dot{w}) dV. \quad (8)$$

Finally, the kinematic equation of sandwich plates subjected to a moving load ( $F$ ) can be formulated as follows:

$$\begin{cases}
 \frac{\partial N_{xx}}{\partial x} + \frac{\partial N_{xy}}{\partial y} = I_0 \left( \frac{\partial^2 u}{\partial t^2} \right) + I_1 \left( \frac{\partial^2 \theta_x}{\partial t^2} \right), \\
 \frac{\partial N_{xy}}{\partial x} + \frac{\partial N_{yy}}{\partial y} = I_0 \left( \frac{\partial^2 v}{\partial t^2} \right) + I_1 \left( \frac{\partial^2 \theta_y}{\partial t^2} \right), \\
 \frac{\partial Q_x}{\partial x} + \frac{\partial Q_y}{\partial y} + N(w) - F\bar{\delta}(x - x_0) - K_w w + K_s \left( \frac{\partial^2 w}{\partial x^2} + \frac{\partial^2 w}{\partial y^2} \right) = I_0 \left( \frac{\partial^2 w}{\partial t^2} \right), \\
 \frac{\partial M_{xx}}{\partial x} + \frac{\partial M_{xy}}{\partial y} - Q_x = I_1 \left( \frac{\partial^2 u}{\partial t^2} \right) + I_2 \left( \frac{\partial^2 \theta_x}{\partial t^2} \right), \\
 \frac{\partial M_{xy}}{\partial x} + \frac{\partial M_{yy}}{\partial y} - Q_y = I_1 \left( \frac{\partial^2 v}{\partial t^2} \right) + I_2 \left( \frac{\partial^2 \theta_y}{\partial t^2} \right).
 \end{cases} \tag{9}$$

$$N(w) = N_{xx} \frac{\partial^2 w}{\partial x^2} + 2N_{xy} \frac{\partial^2 w}{\partial x \partial y} + N_{yy} \frac{\partial^2 w}{\partial y^2},$$

where  $N(w)$  depicts the nonlinear term,  $K_w$  is the Winkler foundation modulus, and  $K_s$  is the Pasternak shear foundation, and  $\bar{\delta}$  is the Dirac function specify the moving line force position with an assigned velocity along the  $x$ -axis, and;

### 3 Numerical methods

The kinetic dynamic relaxation scheme accompanied by Newmark integral technique are recruited in the study for solving Eq. (9).

$$I = \int_{\frac{h_c}{2}}^{\frac{h_c}{2} + h_f} \rho_f(z^0, z^1, z^2) dz + \int_{-\frac{h_c}{2}}^{\frac{h_c}{2}} \rho_c(x, z)(z^0, z^1, z^2) dz + \int_{-\frac{h_c}{2}}^{-\left(\frac{h_c}{2} + h_f\right)} \rho_f(z^0, z^1, z^2) dz. \tag{10}$$

Three set of boundary constrains, namely simply supported boundary conditions, SCSC and clamped boundary condition and, are considered for the completion of the derived equations.

#### 3.1 Newmark integration method

On the basis of Newmark approach, the first and second derivatives of  $\mathbf{x}$  at the next time period,  $t_{j+1}$ , are defined as:

(a) Fully simply supported boundary edge (SSSS)

$$\begin{cases}
 x = 0, a \rightarrow u = v = w = \psi_y = M_{xx} = 0 \\
 y = 0, b \rightarrow u = v = w = \psi_x = M_{yy} = 0
 \end{cases} \tag{11}$$

$$\dot{\mathbf{x}}_{j+1} = \left( \frac{\gamma}{\beta \Delta t_j} (\mathbf{x}_{j+1} - \mathbf{x}_j) - \left( \frac{\gamma}{\beta} - 1 \right) \dot{\mathbf{x}}_j - \left( \frac{\gamma}{2\beta} - 1 \right) \Delta t_j \ddot{\mathbf{x}}_j \right), \tag{14}$$

(b) Parallel edges are simply supported and clamped (SCSC)

$$\begin{cases}
 x = 0, a \rightarrow u = v = w = \psi_y = M_{xx} = 0 \\
 y = 0, b \rightarrow u = v = w = \psi_x = \psi_y = 0
 \end{cases} \tag{12}$$

$$\ddot{\mathbf{x}}_{j+1} = \left( \frac{1}{\beta (\Delta t_j)^2} (\mathbf{x}_{j+1} - \mathbf{x}_j) - \frac{1}{\beta \Delta t_j} \dot{\mathbf{x}}_j - \left( \frac{1}{2\beta} - 1 \right) \ddot{\mathbf{x}}_j \right), \tag{15}$$

in which,  $\mathbf{x}$  is the displacement field of the nanoplate ( $\mathbf{x} = \mathbf{u}, \mathbf{v}, \mathbf{w}, \boldsymbol{\psi}_x, \boldsymbol{\psi}_y$ ),  $\Delta t$  is real time interval,  $\gamma$  and  $\beta$  are Newmark's coefficients. By substituting Eqs. (14) and (15) into Eq. (9), it gives:

(c) Fully clamped boundary edge (CCCC)

$$\begin{cases}
 x = 0, a \rightarrow u = v = w = \psi_x = \psi_y = 0 \\
 y = 0, b \rightarrow u = v = w = \psi_x = \psi_y = 0
 \end{cases} \tag{13}$$

$$[\bar{\mathbf{K}}_{j+1}] \mathbf{x}_{j+1} = \{\bar{\mathbf{P}}_{j+1}\}, \tag{16}$$

in which  $[\bar{\mathbf{K}}_{j+1}]$  is the corresponding stiffness matrix and  $\{\bar{\mathbf{P}}_{j+1}\}$  represents corresponding load vector, defined as:

$$[\bar{\mathbf{K}}_{j+1}] = \frac{1}{\beta (\Delta t_j)^2} [\mathbf{I}_{j+1}] + [\mathbf{K}_{j+1}] \tag{17}$$

$$\{\bar{\mathbf{P}}_{j+1}\} = \{\mathbf{P}(t_{j+1})\} + \left\{ [\mathbf{I}_{j+1}] \left[ \frac{1}{\beta(\Delta t_j)^2} \mathbf{x}_j + \frac{1}{\beta \Delta t_j} \dot{\mathbf{x}}_j + \left( \frac{1}{2\beta} - 1 \right) \ddot{\mathbf{x}}_j \right] \right\}, \tag{18}$$

where  $[\mathbf{I}_{j+1}]$  is the mass matrix and  $[\mathbf{K}_{j+1}]$  represents the stiffness matrix. Also,  $\{\mathbf{P}_{j+1}\}$  denotes the external work vector.

### 3.2 Kinetic dynamic relaxation technique

Equation (9) can be solved when it is transformed into fictitious dynamic space by artificial inertia matrix  $[\mathbf{M}]_{\text{DR}}$  as follows [36]:

$$[\mathbf{M}]_{\text{DR}}^n \{\mathbf{a}\}^n + [\bar{\mathbf{K}}_{j+1}]^n \mathbf{x}_{j+1}^n = \{\bar{\mathbf{P}}_{j+1}^n\}, \tag{19}$$

where  $\{\mathbf{a}\}^n$  and  $[\mathbf{M}]_{\text{DR}}^n$  denote, respectively, the fictitious acceleration vector in  $n$ th iteration of the Kinetic DR [36] and diagonal artificial mass matrix. A proper fictitious mass can guarantee the convergence of K-DR technique. Such an artificial mass is defined in accordance with the Gershgorin theorem [37].

$$m_{ii}^{\text{DOF}} \geq 0.5(\tau^n)^2 \sum_{p=1}^{\text{DOF}} |k_{ip}|, \quad k_{ip} = \frac{\partial \{[\bar{\mathbf{K}}_{j+1}]^n x_{j+1}^n\}}{\partial x}, \tag{20}$$

in which  $m_{ii}$  and DOF are, respectively, fictitious mass matrix elements and the number of degrees of freedom. Nodal velocity and displacement vectors at the next fictitious time stage,  $\tau$ , can be stated by:

$$\{\mathbf{v}\}^{n+1/2} = \mathbf{v}^{n-1/2} + \frac{\tau^n}{[\mathbf{M}]_{\text{DR}}} \{\mathbf{R}\}^n, \quad \{\mathbf{R}\}^n = \{\bar{\mathbf{P}}_{j+1}^n - [\bar{\mathbf{K}}_{j+1}]^n \mathbf{x}_{j+1}^n\} \tag{21}$$

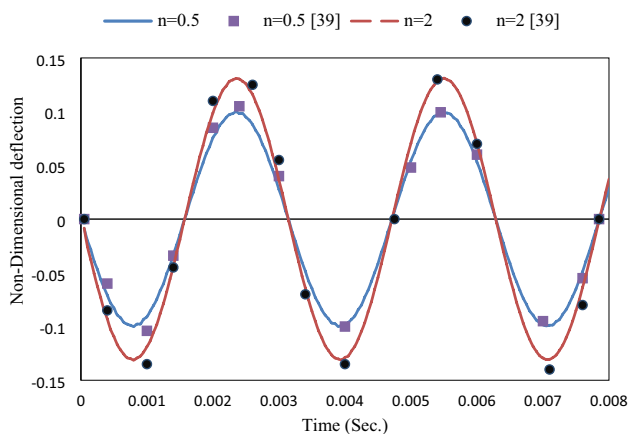


Fig. 3 Time dependent non-dimensional deflection at the center of a clamped square FG plate

$$\{\mathbf{x}\}^{n+1} = \{\mathbf{x}\}^n + \tau^n \{\mathbf{v}\}^{n+1/2}. \tag{22}$$

Furthermore, the kinetic energy of system can be obtained by:

$$\text{KE}^{n+1} = \frac{1}{2} \sum_{i=1}^{\text{DOF}} m_{ii}^n \left( v_i^{n+1/2} \right)^2. \tag{23}$$

As the maximum value of kinetic energy is determined, the K-DR iteration is started again with another novel initial nodal displacement and velocity as follows [38]:

$$\{\mathbf{x}\}^{n-1/2} = \{\mathbf{x}\}^n - \left( \frac{3}{2} \tau^n \right) \{\mathbf{v}\}^{n+1/2} + \frac{(\tau^n)^2}{2[\mathbf{M}]_{\text{DR}}} \{\mathbf{R}\}^n \tag{24}$$

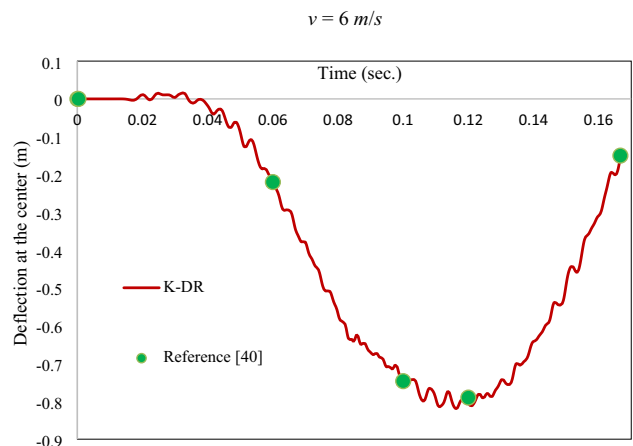


Fig. 4 Vertical displacement at the center of a clamped plate under a traveling force

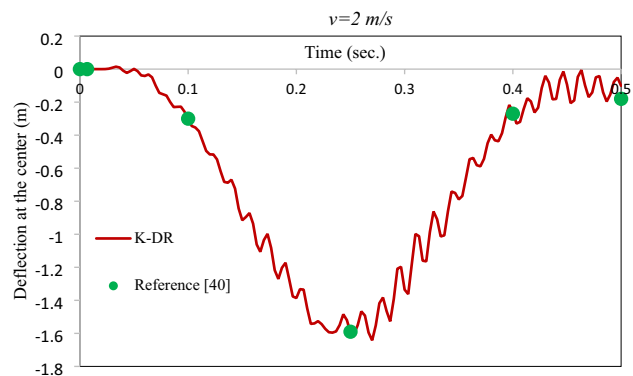


Fig. 5 Vertical displacement at the center of a simply supported plate under a traveling force



**Table 1** Influences of gradient indexes ( $n, m$ ) on the magnitude of  $w_{\max}/h$

	(2, 2)	(2, 4)	(4, 2)	(4, 4)
Current study	2.71	2.85	2.90	3.20
Ref. [20]	2.71	2.85	2.90	3.20

$$\{\mathbf{v}\}^{n+\frac{1}{2}} = \frac{\tau}{2[\mathbf{M}_{DR}]^n} \{\mathbf{R}\}^n. \tag{25}$$

The satisfaction of two criteria (i.e.  $|\mathbf{KE}^{n+1}| \leq 10^{-12}$  and  $|\{\mathbf{R}^n\}| \leq 10^{-9}$ ) leads to stopping the K-DR procedure. These steps are iterated for each time increment of implicit Newmark integration.

## 4 Numerical results

### 4.1 Comparison study

*Case study 1* for the first case, the dynamic response of a 1D-FG plate under a uniform harmonic force,  $F(x, y, t) = 10 \sin(2000t)$  is carried out with the current method, and the obtained results are compared with those reported by [39]. The following properties have been considered:

$$\begin{cases} a = b = 1, h/a = 0.2, \\ E_1 = 70 \text{ GPa}, \rho_1 = 2702 \text{ kg/m}^3, v_1 = 0.3, \\ E_2 = 200 \text{ GPa}, \rho_2 = 5700 \text{ kg/m}^3, v_2 = 0.3. \end{cases} \tag{26}$$

Also  $\bar{w} = \frac{100E_1 h^3 w}{12a^4(1-v_1^2)F_0}$  is defined as the non-dimensional deflection where  $F_0$  represents transverse load applied on the top surface of the plate. Figure 3 reveals a perfect match between the obtained results and those reported in [39].

*Case study 2* in the second example, the transverse displacements at the center of clamped and simply supported plates under action of a moving load are obtained by K-DR method. The parameters used in this example are:

$$\begin{cases} a = b = 1, \rho h/D = 1, F/D = 1 \\ x_0 = vt, y_0 = 1/2 \end{cases} \tag{27}$$

In this sample, the external load,  $F$ , moves on the mid-line of the plate along the  $x$  direction. The bending rigidity of the plate is denoted by  $D$  and  $t$  is the time needed for the load to travel on the plate. From Figs. 4 and 5, a close agreement can be seen between the present results and the reference [40].

*Case study 3* for checking the accuracy of the present formulation and numerical system, the effects variations of vertical ( $n$ ) and axial ( $m$ ) grading indexes on the non-dimensional central deflection of a CCCC bi-dimensional functionally graded plate under a moving load with the velocity of  $v$  are compared in Table 1. The plate has the following geometrical and mechanical features;

$$\begin{aligned} a = b = 1000 \text{ mm}, h_c = 100 \text{ mm} \\ E_1 = 116 \text{ GPa}, \rho_1 = 1200 \text{ kg/m}^3, v_1 = 0.3 \\ E_2 = 200 \text{ GPa}, \rho_2 = 7850 \text{ kg/m}^3, v_2 = 0.3 \\ E_3 = 380 \text{ GPa}, \rho_3 = 3960 \text{ kg/m}^3, v_3 = 0.18, F = 400 \frac{kN}{m}, x_0 = vt. \end{aligned} \tag{28}$$

From Table 1, it can be noticed that the current results are in perfect agreements with those of Ref. [20] which can confirm the accuracy of the methodology and solutions.

### 4.2 Parametric study

The influences of the elastic foundations, porous distributions, material gradient indexes and borderline constrains on dimensionless dynamic central deflection of the sandwich plates with imperfect 2D-FG core are investigated. To do this, a square-shaped three-layer plate with the following geometrical and mechanical properties is considered.

$$\begin{aligned} a = b = 1000 \text{ mm}, h_c = 100 \text{ mm} \\ E_1 = 116 \text{ GPa}, \rho_1 = 1200 \text{ kg/m}^3, v_1 = 0.3 \\ E_2 = 200 \text{ GPa}, \rho_2 = 7850 \text{ kg/m}^3, v_2 = 0.3 \\ E_3 = 380 \text{ GPa}, \rho_3 = 3960 \text{ kg/m}^3, v_3 = 0.3 \\ E_f = 200 \text{ GPa}, \rho_f = 7850 \text{ kg/m}^3, v_f = 0.3. \end{aligned} \tag{29}$$

**Table 2** Effects of elastic foundations and porosity distributions on the supreme amount of deflection of the sandwich plate (SSSS)

$K_s$ (GPa m)	$K_w$ (GPa/m)	$W_{\max}$	
		Even porosity pattern	Uneven porosity pattern
0	0.0	- 1.55	- 1.35
	1.0	- 1.44	- 1.26
0.1	0.0	- 1.23	- 1.12
	1.0	- 1.13	- 1.04

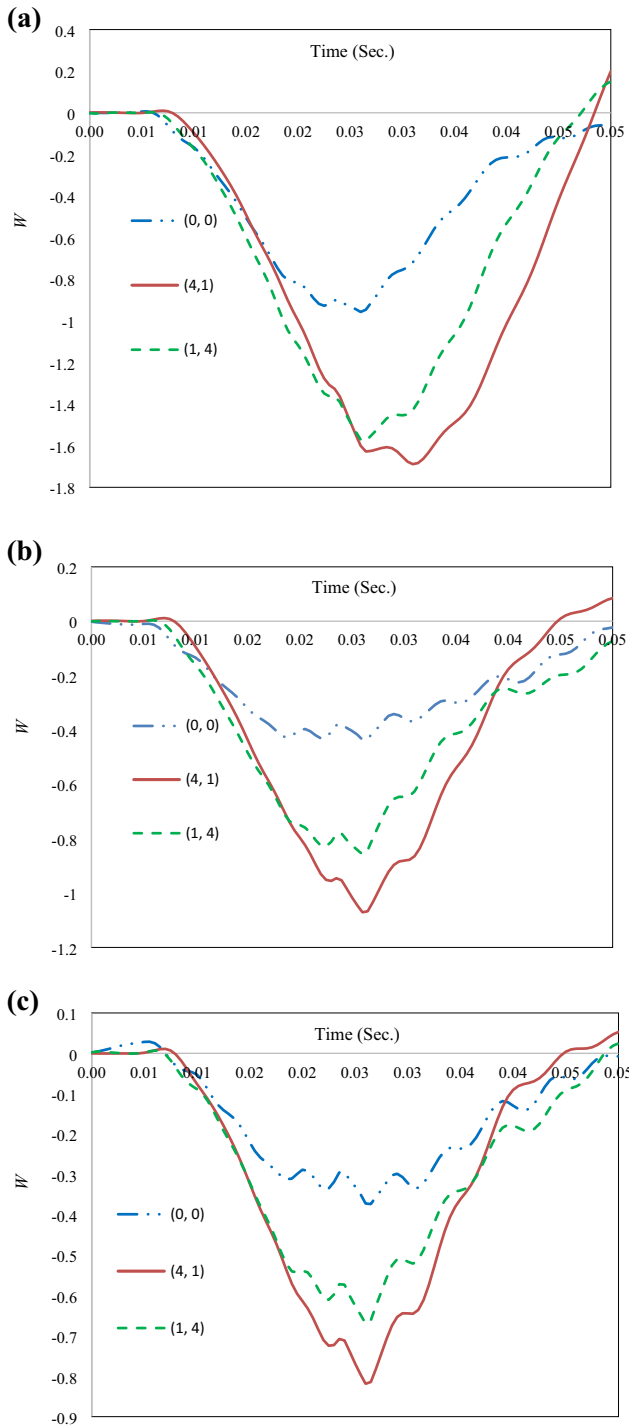


**Fig. 6** Effects of the material gradient indexes  $(n, m)$  on dynamic behavior of the uneven porous 2D-FG sandwich plate; **a** SSSS, **b** SCSC, **c** CCCC

The upper surface of the plate is exposed to a line load travelling along the  $x$  axis with a constant velocity of  $v$ :

$$F = 400 \frac{\text{kN}}{\text{m}}, x_0 = vt \tag{30}$$

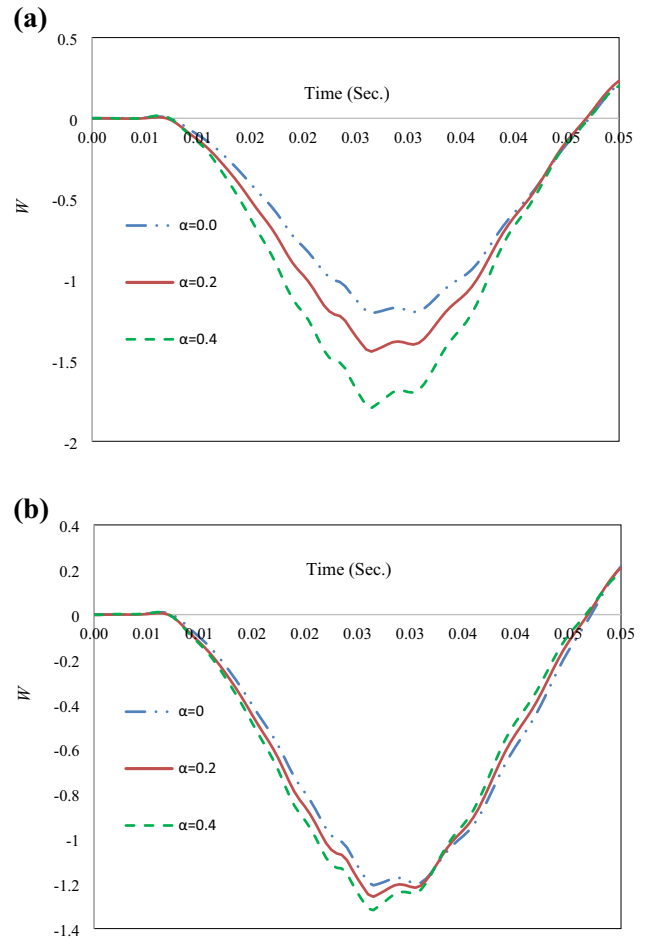


**Fig. 7** Impacts of the porosity coefficients on dynamic behavior of the SSSS sandwich plates; **a** even porosity distribution, **b** uneven porosity distribution ( $n = m = 1$ )

The following dimensionless deflection is used to express results:

$$W = \frac{w(a/2, b/2)}{h_c} \times 1000. \tag{31}$$

Unless mentioned otherwise,  $h_s$ ,  $K_s$  and  $K_w$  are respectively 10 mm, 0.0 GPa m and 1.0 GPa/m, respectively.

Influence of the foundation stiffness on dimensionless central deflection of SSSS sandwich plates subjected to a moving load ( $v = 20$  m/s) for two porous distributions with fraction of 0.2 and  $(n, m) = (1, 1)$  is considered and the resulted magnitudes are provided in Table 2. As depicted in Table 2, the elastic foundations can lead to a considerable decline of the dynamic dislocation in all cases. The plates with even porosity pattern have the largest dynamic deflection of  $-1.55$  when  $K_w = 0$  and  $K_s = 0$ . The deflection of plates resting on an elastic foundation with even and uneven



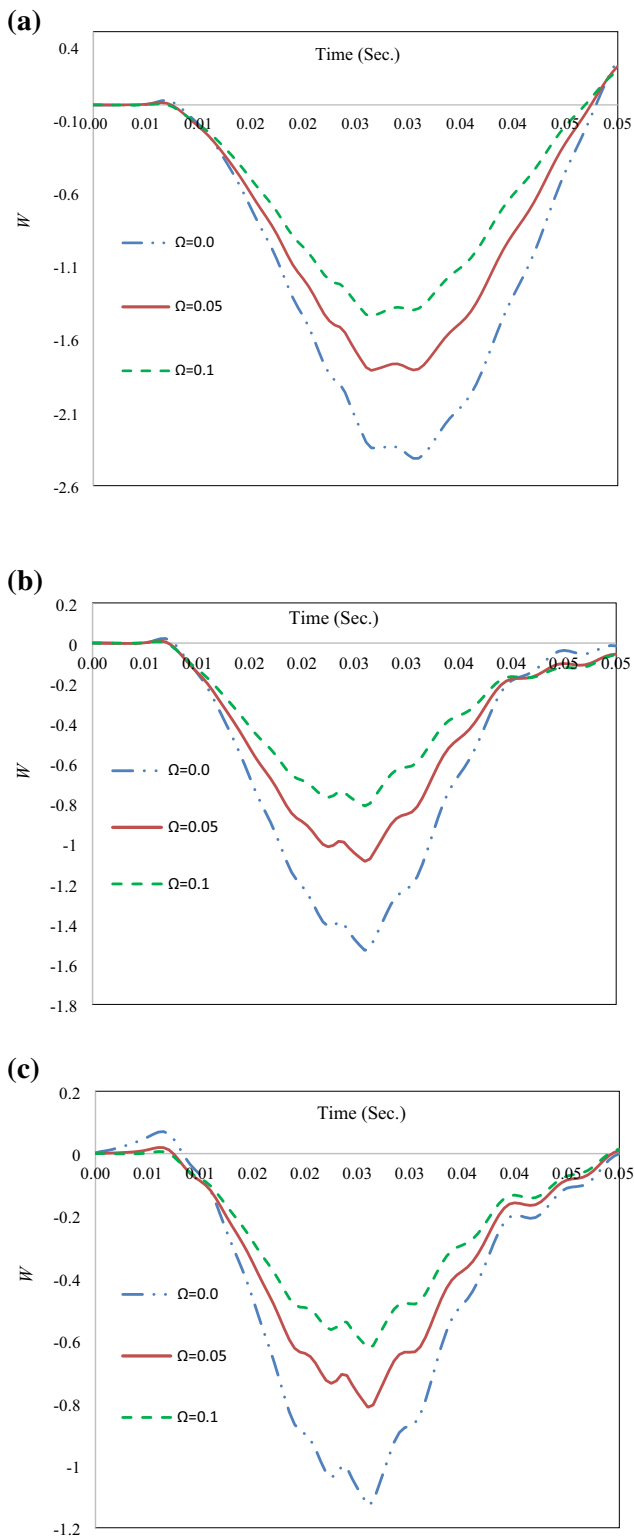


**Fig. 8** Non-dimensional vertical displacement at the center of the 2D-FG sandwich plate with porosity distributed evenly through the thickness exposed to a moving load in various boundary constrains ( $\alpha = 0.2, n = m = 1, v = 20 \text{ m/s}$ ); **a** SSSS, **b** SCSC, **c** CCCC

porous cores as well as  $K_s = 0.1 \text{ GPa m}$  and  $K_w = 1.0 \text{ GPa/m}$   $t$  falls noticeably to  $-1.13$  and  $-1.04$ , respectively.

Figure 6 demonstrates how the material gradient factors ( $n, m$ ) affect the transient vertical displacement of sandwich SSSS, SCSC and CCCC plates with even porous 2D-FG core ( $\alpha = 0.2$ ) under a moving load with a velocity of 20 m/s. For all three sorts of boundary conditions, it is evident that with a rise in the quantity of material gradient indexes ( $n, m$ ), a greater dynamic deflection will be seen since climbing these parameters result in decreasing the bending rigidity of the sandwich plate. It is also seen that the influence of the index ( $n$ ) is much noticeable in comparison with the grading index ( $m$ ) when the plate edges are SCSC and CCCC.

The non-dimensional central deflection of a SSSS sandwich plate subjected to a moving load ( $v = 20 \text{ m/s}$ ) is plotted in Fig. 7 for even and uneven porosity distributions, respectively. It is obvious from Fig. 7 that the dimensionless dynamic displacement of the plates increases with a growth in the values of porosity fractions. In comparison with the uneven distribution, the influence of the imperfection rise is much greater when the plate is defected with even porosity distribution, see Fig. 7a. In this case, the dynamic deflection increases to 0.22 and 0.36 unit by rising the porosity fraction of 0.2 and 0.4, respectively.

Figures 8a–c, respectively, show non-dimensional transient deflection at the center versus different magnitudes of  $\Omega (= h_f/h_c)$  for  $n = m = 1$  with SSSS, SCSC and CCCC boundary conditions, respectively. It is presumed that  $v = 20 \text{ m/s}, \alpha = 0.2$  and porosity distribution is even. From these figures, it is seen that the dynamic deflections decrease remarkably with a rise in the value of  $\Omega$  for every edge constrain. The most significant decreases due to ceramic layers can be shown when  $\Omega$  changes from 0 to 0.05. It is also seen from these figures that SSSS case offers greater effects on the reduction of dimensionless dynamic displacements in all face layer’s thicknesses. For instance, the face layer with depth ratio ( $\Omega$ ) of 0.1 condenses the vertical displacement of the SSSS plate with no face surfaces about 0.98 unit whereas it is 0.718 and 0.507 for the SCSC and CCCC plates, respectively.

### 5 Concluding remarks

The nonlinear transient behavior of sandwich plates with porous 2D-FG cores subjected to moving mechanical loads supported by the elastic foundations with SSSS, SCSC and CCCC boundary surroundings has been explored. Having governed by FSDT along with von Karman nonlinearity, the kinetic equations have been solved by implementing the kinetic dynamic relaxation method coupled with Newmark’s integration approach. In this investigation, two types of porosity distributions have been considered, and the effects

of imperfection distributions and coefficients, parameters of elastic foundation and boundary conditions have been analyzed. From the numerical results, the following conclusions are noticeable:

- Elastic foundations offer more reinforcing effects when plates have imperfections in the even pattern.
- Transient responses of the plates increase with an increment in the magnitudes of porosity fractions; and compared to the structures with even micro-voids, the ones with uneven porosity have the lower bending deformation.
- The dynamic characteristics of the structure are highly influenced by material properties parameters ( $n, m$ ); and the longitudinal functionally graded factor ( $n$ ) has a superior impact on CCCC than SSSS sheets.
- The effect of face layer's thickness on the dynamic response of SSSS plates is more noticeable compared to that of SCSC and CCCC plates. So, it can be said that the impact of the face layer's thickness on the decrease of displacement growths by decreasing constrains on the plate edge surroundings.

**Open Access** This article is licensed under a Creative Commons Attribution 4.0 International License, which permits use, sharing, adaptation, distribution and reproduction in any medium or format, as long as you give appropriate credit to the original author(s) and the source, provide a link to the Creative Commons licence, and indicate if changes were made. The images or other third party material in this article are included in the article's Creative Commons licence, unless indicated otherwise in a credit line to the material. If material is not included in the article's Creative Commons licence and your intended use is not permitted by statutory regulation or exceeds the permitted use, you will need to obtain permission directly from the copyright holder. To view a copy of this licence, visit <http://creativecommons.org/licenses/by/4.0/>.

## References

1. Yoosefian AR, Golmakani ME, Sadeghian M (2019) Nonlinear bending of functionally graded sandwich plates under mechanical and thermal load. *Commun Nonlinear Sci Numer Simul*. <https://doi.org/10.1016/j.cnsns.2019.105161>
2. Karroubi R, Irani-Rahaghi M (2019) Rotating sandwich cylindrical shells with an FGM core and two FGPM layers. Free vibration analysis. *Appl Math Mech Engl Ed* 40(4):563–578. <https://doi.org/10.1007/s10483-019-2469-8>
3. Bodaghi M, Saidi AR (2011) Thermoelastic buckling behavior of thick functionally graded rectangular plates. *Arch Appl Mech* 81(11):1555–1572. <https://doi.org/10.1007/s00419-010-0501-0>
4. Kamarian S, Shakeri M, Yas MH, Bodaghi M, Pourasghar A (2015) Free vibration analysis of functionally graded nanocomposite sandwich beams resting on Pasternak foundation by considering the agglomeration effect of CNTs. *J Sandw Struct Mater* 17(6):632–665. <https://doi.org/10.1177/1099636215590280>
5. van Do T, Nguyen DK, Duc ND, Doan DH, Bui TQ (2017) Analysis of bi-directional functionally graded plates by FEM and a new third-order shear deformation plate theory. *Thin Walled Struct* 119:687–699. <https://doi.org/10.1016/j.tws.2017.07.022>
6. Yuan Y, Zhao K, Sahmani S, Safaei B (2020) Size-dependent shear buckling response of FGM skew nanoplates modeled via different homogenization schemes. *Appl Math Mech Engl Ed* 41(4):587–604. <https://doi.org/10.1007/s10483-020-2600-6>
7. Sahmani S, Aghdam MM, Rabczuk T (2018) Nonlocal strain gradient plate model for nonlinear large-amplitude vibrations of functionally graded porous micro/nano-plates reinforced with GPLs. *Compos Struct* 198:51–62. <https://doi.org/10.1016/j.compstruct.2018.05.031>
8. Nemat-Alla M (2003) Reduction of thermal stresses by developing two-dimensional functionally graded materials. *Int J Solids Struct* 40(26):7339–7356. <https://doi.org/10.1016/j.ijsolstr.2003.08.017>
9. Hasani Baferani A, Saidi AR, Ehteshami H (2011) Accurate solution for free vibration analysis of functionally graded thick rectangular plates resting on elastic foundation. *Compos Struct* 93(7):1842–1853. <https://doi.org/10.1016/j.compstruct.2011.01.020>
10. Sheikholeslami SA, Saidi AR (2013) Vibration analysis of functionally graded rectangular plates resting on elastic foundation using higher-order shear and normal deformable plate theory. *Compos Struct* 106(3):350–361. <https://doi.org/10.1016/j.compstruct.2013.06.016>
11. Chen M, Jin G, Ma X, Zhang Y, Ye T, Liu Z (2018) Vibration analysis for sector cylindrical shells with bi-directional functionally graded materials and elastically restrained edges. *Compos B Eng* 153:346–363. <https://doi.org/10.1016/j.compositesb.2018.08.129>
12. Nguyen T-T, Lee J (2018) Flexural-torsional vibration and buckling of thin-walled bi-directional functionally graded beams. *Compos B Eng* 154:351–362. <https://doi.org/10.1016/j.compositesb.2018.08.069>
13. Fariborz J, Batra RC (2019) Free vibration of bi-directional functionally graded material circular beams using shear deformation theory employing logarithmic function of radius. *Compos Struct* 210:217–230. <https://doi.org/10.1016/j.compstruct.2018.11.036>
14. Tang Y, Ding Q (2019) Nonlinear vibration analysis of a bi-directional functionally graded beam under hygro-thermal loads. *Compos Struct* 225:111076. <https://doi.org/10.1016/j.compstruct.2019.111076>
15. Attia MA, Mohamed SA (2020) Thermal vibration characteristics of pre/post-buckled bi-directional functionally graded tapered microbeams based on modified couple stress Reddy beam theory. *Eng Comput* 75(3):54. <https://doi.org/10.1007/s00366-020-01188-4>
16. Saini R, Lal R (2020) Axisymmetric vibrations of temperature-dependent functionally graded moderately thick circular plates with two-dimensional material and temperature distribution. *Eng Comput* 34(2018):3. <https://doi.org/10.1007/s00366-020-01056-1>
17. Kieback B, Neubrand A, Riedel H (2003) Processing techniques for functionally graded materials. *Mater Sci Eng A* 362(1–2):81–106. [https://doi.org/10.1016/S0921-5093\(03\)00578-1](https://doi.org/10.1016/S0921-5093(03)00578-1)
18. Wang Y, Ye C, Zu JW (2018) Identifying the temperature effect on the vibrations of functionally graded cylindrical shells with porosities. *Appl Math Mech Engl Ed* 39(11):1587–1604. <https://doi.org/10.1007/s10483-018-2388-6>
19. Zhou K, Huang X, Tian J, Hua H (2018) Vibration and flutter analysis of supersonic porous functionally graded material plates with temperature gradient and resting on elastic foundation. *Compos Struct* 204:63–79. <https://doi.org/10.1016/j.compstruct.2018.07.057>
20. Esmaeilzadeh M, Kadkhodayan M (2019) Dynamic analysis of stiffened bi-directional functionally graded plates with porosities

- under a moving load by dynamic relaxation method with kinetic damping. *Aerosp Sci Technol* 93:105333. <https://doi.org/10.1016/j.ast.2019.105333>
21. Esmailzadeh M, Kadkhodayan M, Mohammadi S, Turvey GJ (2020) Nonlinear dynamic analysis of moving bilayer plates resting on elastic foundations. *Appl Math Mech Engl Ed* 41(3):439–458. <https://doi.org/10.1007/s10483-020-2587-8>
  22. Baferani AH, Saidi AR (2013) Effects of in-plane loads on vibration of laminated thick rectangular plates resting on elastic foundation. An exact analytical approach. *Eur J Mech A Solids* 42(7):299–314. <https://doi.org/10.1016/j.euromechsol.2013.07.001>
  23. Gao K, Gao W, Di W, Song C (2017) Nonlinear dynamic characteristics and stability of composite orthotropic plate on elastic foundation under thermal environment. *Compos Struct* 168:619–632. <https://doi.org/10.1016/j.compstruct.2017.02.054>
  24. Şimşek M, Aydın M (2017) Size-dependent forced vibration of an imperfect functionally graded (FG) microplate with porosities subjected to a moving load using the modified couple stress theory. *Compos Struct* 160:408–421. <https://doi.org/10.1016/j.compstruct.2016.10.034>
  25. Yang Y, Kunpang K, Lam C, Iu V (2019) Dynamic behaviors of tapered bi-directional functionally graded beams with various boundary conditions under action of a moving harmonic load. *Eng Anal Bound Elem* 104:225–239. <https://doi.org/10.1016/j.enganabound.2019.03.022>
  26. Golzari A, Asgari M (2018) Dynamic analysis and wave propagation in rotating heterogeneous cylinders under moving load and thermal conditions; implementing an efficient mesh free method. *Appl Math Model* 61:377–407. <https://doi.org/10.1016/j.apm.2018.05.001>
  27. Esmailzadeh M, Kadkhodayan M (2018) Nonlinear dynamic analysis of an axially moving porous FG plate subjected to a local force with kinetic dynamic relaxation method. *Comput Methods Mater Sci* 18(1):18–28
  28. Şimşek M (2010) Vibration analysis of a single-walled carbon nanotube under action of a moving harmonic load based on non-local elasticity theory. *Phys E* 43(1):182–191. <https://doi.org/10.1016/j.physe.2010.07.003>
  29. Chang T-P (2013) Stochastic FEM on nonlinear vibration of fluid-loaded double-walled carbon nanotubes subjected to a moving load based on nonlocal elasticity theory. *Compos B Eng* 54:391–399. <https://doi.org/10.1016/j.compositesb.2013.06.012>
  30. Nami MR, Janghorban M (2015) Dynamic analysis of isotropic nanoplates subjected to moving load using state-space method based on nonlocal second order plate theory. *J Mech Sci Technol* 29(6):2423–2426. <https://doi.org/10.1007/s12206-015-0539-6>
  31. Shahsavari D, Janghorban M (2017) Bending and shearing responses for dynamic analysis of single-layer graphene sheets under moving load. *J Braz Soc Mech Sci Eng* 39(10):3849–3861. <https://doi.org/10.1007/s40430-017-0863-0>
  32. Barati MR, Faleh NM, Zenkour AM (2018) Dynamic response of nanobeams subjected to moving nanoparticles and hygro-thermal environments based on nonlocal strain gradient theory. *Mech Adv Mater Struct* 26(19):1661–1669. <https://doi.org/10.1080/15376494.2018.1444234>
  33. Pirmoradian M, Torkan E, Abdali N, Hashemian M, Toghraie D (2019) Thermo-mechanical stability of single-layered graphene sheets embedded in an elastic medium under action of a moving nanoparticle. *Mech Mater*. <https://doi.org/10.1016/j.mechmat.2019.103248>
  34. Reddy JN (2003) *Mechanics of laminated composite plates and shells*. CRC Press, Boca Raton
  35. Li Q, Di W, Chen X, Liu L, Yu Y, Gao W (2018) Nonlinear vibration and dynamic buckling analyses of sandwich functionally graded porous plate with graphene platelet reinforcement resting on Winkler–Pasternak elastic foundation. *Int J Mech Sci* 148:596–610. <https://doi.org/10.1016/j.ijmecsci.2018.09.020>
  36. Alamatian J (2012) A new formulation for fictitious mass of the dynamic relaxation method with kinetic damping. *Comput Struct* 90–91:42–54. <https://doi.org/10.1016/j.compstruc.2011.10.010>
  37. Lee KS, Han SE, Park T (2011) A simple explicit arc-length method using the dynamic relaxation method with kinetic damping. *Comput Struct* 89(1–2):216–233. <https://doi.org/10.1016/j.compstruc.2010.09.006>
  38. Alic V, Persson K (2016) Form finding with dynamic relaxation and isogeometric membrane elements. *Comput Methods Appl Mech Eng* 300:734–747. <https://doi.org/10.1016/j.cma.2015.12.009>
  39. Rezaei Mojdehi A, Darvizeh A, Basti A, Rajabi H (2011) Three dimensional static and dynamic analysis of thick functionally graded plates by the meshless local Petrov-Galerkin (MLPG) method. *Eng Anal Bound Elem* 35(11):1168–1180. <https://doi.org/10.1016/j.enganabound.2011.05.011>
  40. Eftekhari SA (2015) A differential quadrature procedure with regularization of the dirac-delta function for numerical solution of moving load problem. *Lat Am J Solids Struct* 12(7):1241–1265. <https://doi.org/10.1590/1679-78251417>